Received: 25 January 2024 | Revised: 19 March 2024 | Accepted: 16 April 2024

DOI: 10.1002/jrs.6674

RESEARCH ARTICLE

Journal of RAMAN SPECTROSCOPY WILEY

The *p*H effects on thermal amyloid fibrillation kinetics of hen egg-white lysozyme using new normalization factor for Raman spectroscopy

Dongxiao Liu[1] | **Ning Chen**[1] | **Tianle Zhang**[1] | **Xiaoguo Zhou**[1,2] | **Shilin Liu**[1,2]

[1]Department of Chemical Physics, University of Science and Technology of China, Hefei, China

[2]Hefei National Research Center for Physical Sciences at the Microscale, University of Science and Technology of China, Hefei, China

Correspondence
Xiaoguo Zhou and Shilin Liu, Department of Chemical Physics, University of Science and Technology of China, Hefei 230026, China.
Email: xzhou@ustc.edu.cn and slliu@ustc.edu.cn

Funding information
National Natural Science Foundation of China, Grant/Award Numbers: 22073088, 22027801; National Key Research and Development Program of China, Grant/Award Number: 2022YFF0707202

Abstract

Amyloid fibrillation kinetics of proteins associated with neurodegenerative diseases has been extensively studied using Raman spectroscopy. The normalization factor for the spectra is crucial for obtaining correct kinetics of Raman indicators, especially vibrational band intensities. Here, we compared the concentration dependences between the absorption at 280 nm in UV–vis spectroscopy and the phenylalanine (Phe) Raman band intensity at 1003 cm^{-1} in amyloid fibrillation kinetics of lysozyme. The former exhibits better performance as normalization factor. Using this new normalization factor, the effect of *p*H value on the transformation of hen egg-white lysozyme (HEWL) tertiary and secondary structures was studied subsequently. With increasing acidity, the unfolding of tertiary structures and the transformation of secondary structures are significantly accelerated. Notably, the populations of various secondary structures in the final state remain in the *p*H < 2.0 solutions, indicating that the branching ratios of "on-pathway" to amyloid fibrils and "off-pathway" to gel-like aggregates are independent on the *p*H value in the range of 1.1–1.9.

KEYWORDS

amyloid fibrillation, lysozyme, *p*H effect, Raman spectroscopy

1 | INTRODUCTION

Specific functions of proteins in living organisms are associated with their unique structures. In some specific conditions, proteins can undergo denaturation and self-assembly to form amyloid fibrils, thereby causing some human neurodegenerative diseases.[1–3] During past decades, various kinetics of protein amyloid fibrillation have been investigated with thermal and acid treatments,[4–7] additions of metal ions such as Zn^{2+},[8] Cu^{2+},[9,10] Fe^{3+},[11] and Mn^{2+}.[12,13]

Among these studies, hen egg-white lysozyme (HEWL) has been most widely used as a model globular protein because of its association with hereditary systemic amyloidosis in humans.[14–18] HEWL has 129 amino acid residues and consists of two structural domains, α (Lys1-Asn39, Ser86-Leu129) and β (Thr40-Ser85), including six Trp, three Tyr, and three Phe residues. HEWL has a molecular weight of approximately 14.3 kDa and a predominantly α-helical conformation (~45%) in native state, and its structural stability in aqueous solutions is mainly through hydrophobic interactions and hydrogen bonding. Thus, the *p*H value can severely affect protein structural stability in aqueous solutions in principle. Al Adem et al. used ThT fluorescence spectroscopy and transmission electron microscopy to characterize the

HEWL aggregates formed in acidic (*p*H 3) and physiological (*p*H 7.4) environments.[19] They found that nonfibrous aggregates dominated at *p*H 7.4, whereas fibrils were slowly formed at *p*H 3.0. Venkataramani et al.[20] and Lewis et al.[21] verified that the significant transformation of HEWL secondary structures only occurred at *p*H < 2, and the denaturation temperature tended to be lower under more acidic conditions, by means of Fourier transform infrared (FTIR) spectroscopy, dynamic light scattering, and Raman spectroscopy. However, only a few *p*H conditions were measured previously, such as *p*H 2, 3, 4, 7, and 12.[22,23] Especially, within the *p*H range of less than 2.0, no systematic study has been performed to study the *p*H-dependent kinetics of protein tertiary and secondary structure transformation to date. Therefore, it is insufficient to in-depth understand the HEWL denaturation mechanism with the action of acids.

Many experimental techniques have been successfully applied to identify and separate protein aggregates formed in the amyloid fibrillation kinetics of HEWL, based on imaging, scattering, spectroscopy, and calorimetric methods.[24] Among these techniques, Raman spectroscopy shows a unique and powerful ability to achieve detailed information of protein conformational transformations.[25–29] A number of Raman indicators have been summarized in Table 1, such as peak intensities, Raman shifts, full width at half maximum (FWHM) of specific vibrational bands, and even intensity ratios of correlated peaks (e.g., I_{1340}/I_{1360}).[38] These indicators are generally sensitive to protein tertiary and secondary structures,[39] and hence, their evolution kinetics can accurately reflect the information of structural changes during protein denaturation processes.

To accurately monitor the time-dependent changes of the above indicators, especially those of peak intensity, normalization of Raman spectra is one of the crucial data-processing steps, as the protein denaturation is usually accompanied by the significant change of protein concentration due to aggregation and precipitation processes. A previous investigation proposed that the peak intensity of Phe band at 1003 cm^{-1} was insensitive to micro-environment and exclusively depended on the protein concentration.[40] Consequently, it has been used as the normalization factor of Raman intensities.[41–43] However, using high-resolution Raman vibrational spectroscopy, Xing et al. observed an obviously broadened bandwidth of this indicator in HEWL amyloid formation kinetics with thermal and acidic treatment,[44] implying that the presupposed consistence between the protein concentration and the Phe intensity could be questioned.

Herein, we re-investigate the relationships between the Phe band intensity and the HEWL concentration with thermal and acidic treatments (65°C and *p*H 1.9). In contrast, the UV–vis absorption spectroscopy of protein is recorded simultaneously. By comparing the kinetic curves of the Phe band intensity, the UV–vis absorbance at 280 nm, and the protein concentration in supernatants, the absorbance at 280 nm exhibits the best consistence with the protein concentration and thus can be used as a more appropriate normalization factor for Raman spectroscopy. Subsequently, Raman spectroscopic analyses are conducted for the HEWL aqueous solution in thermal amyloid fibrillation kinetics under three acidic conditions of *p*H = 1.1, 1.9, and 2.7, using this new normalization factor. The specific *p*H effects on the evolution kinetics of the HEWL secondary and tertiary structures are unraveled.

TABLE 1 The commonly used Raman indicators for the HEWL in aqueous solutions.

Groups	Raman shift/cm^{-1}[1a]	Assignment	Raman indicator
S-S	508 (511)	Stretching of disulfide bond	Intensity[30]
Trp	759 (759)	Coupled vibrations of in-phase breathings of benzene and pyrrole	Intensity[30,31]
N-C_α-C	932 (935)	Stretching of N-C_α-C in the α-helical structure	Intensity[32–35]
Phe	1003 (1003)	Ring breathing of benzene in the Phe amino residue	FWHM[33,34]
Trp	1340 & 1360 (1340 & 1360)	Fermi resonances between the fundamental in-plane N1 = C8 stretching and combination bands of ring out-of-plane deformations	Intensity ratio I_{1340}/I_{1360}[32,36]
Amide I	1658 (1671)	The coupling mode of the C=O and C-N stretching vibration and a small amount of N-H in-plane bending vibration	Peak position[34,37]

[a]The values in parentheses are the Raman shifts of the mature fibrils.

2 | EXPERIMENTAL

2.1 | Solution preparation

HEWL was purchased from Sangon Biotech (Shanghai) Co. Ltd. and was used without further purification. Similar to the previous studies,[15,18,45] amyloid fibrillation of the lysozyme aqueous solution was conducted in thermal and acidic conditions, where the *p*H values of solution were respectively adjusted to 1.1, 1.9, and 2.7 by adding hydrochloric acid. The lysozyme solution with an initial concentration of 20 mg/mL was sealed in twenty 5-mL glass vials and then was incubated in a thermoshaker incubator at 65°C without agitation. At each specific incubation time, one vial of the protein solution was taken out and centrifuged at 12,000 g for 20 min to separate supernatant and insoluble aggregates. The supernatant was directly used for Raman and UV–vis absorption spectroscopy assays, while the insoluble phase was dried and weighed.

2.2 | Raman spectroscopy

Spontaneous Raman scattering spectroscopy was performed as described previously.[44,46,47] A continuous-wave laser (Verdi V5, 532 nm, Coherent) with the power of 5 W was used as an excitation laser, and the Raman light was collected and dispersed by a triple monochromator (Triple-Pro, Acton Research) equipped with a liquid-nitrogen-cooled CCD detector (Spec-10:100B, Princeton Instruments). The acquisition time for recording each spectrum was 20 s, and the identical measurements were repeated for 15 times in same conditions. As a result, the averaged Raman spectra at each incubation time were achieved with better signal-to-noise ratios. Moreover, the spectrum of hydrochloric acid solution was measured in identical conditions as the background (in Figure S3), and the reported Raman spectra of protein were modified by subtracting the background and then being normalized to eliminate the influences of protein concentration, where the available normalization factor was discussed in the following sections. In current experiments, the resolution of Raman spectra was ~1 cm^{-1}. The Raman shifts were calibrated using the standard spectral lines of a mercury lamp. Notably, as confirmed in our previous experiments with the confocal micro-Raman spectrometer,[44] Raman spectra of the supernatant after incubation for more than 200 h were almost identical to those of the gelation after lyophilization. Consequently, Raman spectroscopy assay of the supernatants can exhibit the conformational transformation of protein secondary and tertiary structures.

2.3 | Ultraviolet–visible absorption spectrum

A commercial UV–vis spectrometer (UV-2550, Shimadzu) was used to measure UV–visible absorption spectra of the supernatant at each incubation time in the wavelength range of 200–500 nm. To avoid saturation absorption caused by excessive concentrations of proteins, the supernatant was diluted 20 times prior to spectroscopy assays. Dilutions and spectra measurements were done at room temperature.

3 | RESULTS AND DISCUSSION

3.1 | Accurate determination of lysozyme concentration in supernatant

In thermal and acidic conditions, proteins can self-assemble into aggregates such as amyloid fibrils and gels.[48–50] Considering the low solubility of these aggregates, the protein concentration in the incubated solution is significantly reduced with time. By weighing the masses of protein solution and precipitate at each incubation time, we can calculate the concentration of lysozyme in the supernatant using the following Equations (1) and (2).

$$C_t = [C_0 \cdot V_0 - m_s(t)]/V_t \quad (1)$$

$$V_t = V_0 - (m_0 - m_t)/\rho_{H2O} \quad (2)$$

where C_0 and C_t, m_0 and m_t are the protein concentrations (in the unit of mg/mL) and the total masses of solution (in mg) at the initial and specific incubation times, respectively, and $m_s(t)$ is the mass of precipitate (in mg) after centrifugation and drying at a certain incubation time, V_0 (= 5 mL) and V_t are the solution volume before and after incubation, and ρ_{H2O} (= 997.048 mg/mL) is the density of the solvent water at 25°C. Notably, it was found that small amounts of solvent water evaporate during the incubation period, leading to the slight reduction of solution volume and mass, which needs to be calibrated with Equation (2).

The incubation time-dependent concentration of the protein in the supernatant at *p*H 1.9 is exhibited in Figure 1. Obviously, there is a lag phase followed by a monotonically attenuation. The lag duration is approximately 21 h in the current conditions, implying that oligomers formed at the early stage are soluble, whereas insoluble aggregates are produced after incubation for ~21 h, which generally agrees with the previous AFM conclusions.[44]

3.2 | Variation of the absorbance at 280 nm during the HEWL amyloid fibrillation

UV–visible absorption spectroscopy is a commonly used method for protein analysis.[51–54] In HEWL, the amino acid residues with aromatic rings, such as Trp, Phe, and Tyr, have remarkable absorptions in the near UV wavelength region, for example, the molar extinction coefficients (ε) are 5.59×10^3 L·mol^{-1}·cm^{-1} for Trp monomer at 278 nm, 1.36×10^3 L·mol^{-1}·cm^{-1} for Tyr at 274 nm, and 0.20×10^3 L·mol^{-1}·cm^{-1} for Phe at 258 nm. Figure 2A shows the UV–visible absorption spectra of the lysozyme aqueous solution at *p*H 1.9 in the native state and the final state after incubation for 196 h, as well as those of three amino acid monomers. In the wavelength range of 240–700 nm, a unique absorption with the center at 280 nm is observed for the native HEWL and the incubated protein, and moreover, its profile is virtually unchanged except for a marked decrease in intensity. Compared with the spectra of amino acid monomers, the absorption band at 280 nm of the protein is mostly contributed by Trp and Tyr residues. In addition, accompanying with the protein denaturation, the absorbance at 280 nm decreased significantly.

Figure 2B shows the variation curve of the absorbance at exact 280 nm of the supernatant at *p*H 1.9 during amyloid fibrillation process, as well as that of the protein concentration. The perfectly consistent curves indicate that the absorbance at 280 nm exclusively depends on the protein concentration during amyloid fibrillation process and is insensitive to conformational changes of lysozyme. In other words, this absorbance is an excellent normalization factor for the protein concentration when comparing Raman spectra of denaturing proteins.

To access the versatility of this normalization factor, we conducted an additional experiment with a lower initial concentration of protein (2 mg/mL), where the other experimental conditions were identical, such as *p*H value, incubation temperature, and volume of glass vial. Although the aggregation pathways of HEWL were slightly changed because of the concentration effect under these conditions, a great consistence was also obtained for the concentration and the absorbance, providing solid evidence for the generality of this normalization factor. The additional experimental results are shown in Figures S1 and S2.

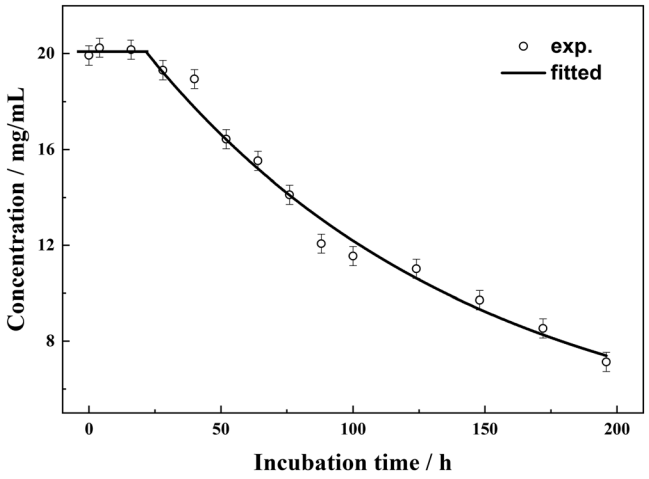

FIGURE 1 Time-dependence of the protein concentration in the supernatant at *p*H 1.9 during the thermal incubation.

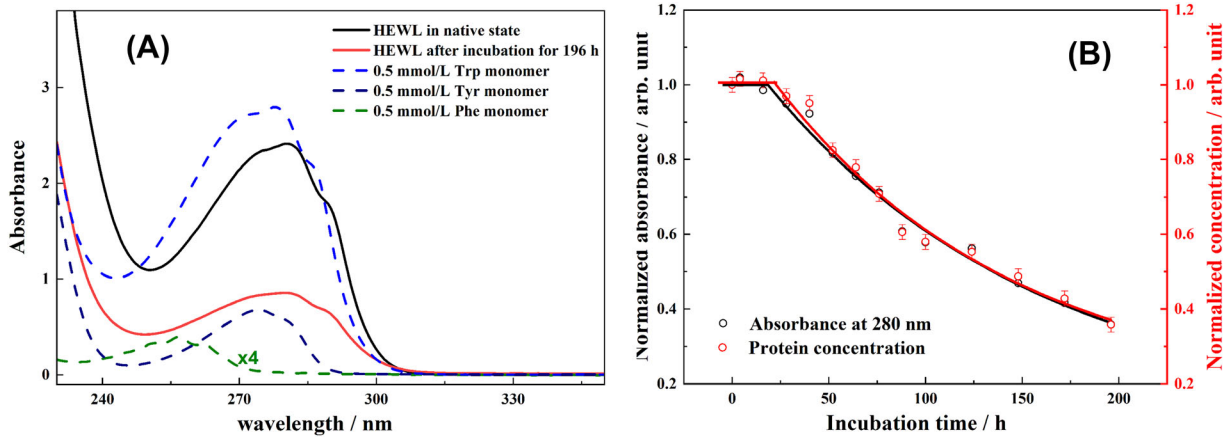

FIGURE 2 (A) UV–vis absorption spectra of the HEWL aqueous solution at *p*H 1.9 in the native state (in black) and the final state after incubation for 196 h (in red), as well as those of Trp, Phe, and Tyr amino acid monomers with the concentration of 0.5×10^{-3} mol·L^{-1}; (B) time-dependent curve of the normalized absorbance at 280 nm in UV–vis absorption spectra (in black) and the normalized concentration of the supernatant solution (in red) during thermal incubation at *p*H 1.9.

3.3 | Evolution kinetics of the Phe peak at 1003 cm^{-1} in Raman spectra

Figure 3 shows the recorded Raman spectra of HEWL in the native state and the final state after incubation for 196 h with thermal and acidic treatments (65°C, *p*H 1.9). Obviously, all peak intensities are apparently reduced after incubation because of the formation of aggregates. Additionally, a peak position shift of the amide I band, as well as the increase of the intensity ratio, I_{1340}/I_{1360}, is obviously visible after incubation, indicating the transformation of protein structures.

To verify the reliability of the Phe band intensity as normalization factor, we compared its evolution kinetics with the protein concentration. Considering that there are three overlapped peaks in the range of 990–1040 cm^{-1} as shown in the partially magnified Raman spectrum of Figure 4A,B, we used three-peak fitting to achieve the individual profile of the Phe peak centered at 1003 cm^{-1}. A slightly increased FWHM of the peak was observed from 3.2 cm^{-1} in the native state to 3.7 cm^{-1} in the final state after incubation, in line with the unfolding of protein tertiary structures and previous conclusions.[44] Moreover, the temperature-dependent behavior of this FWHM was reported to be a typical sigmodal curve.[39] Notably, the change trends in Figure 4C,D are inconsistent with that of protein concentration, thereby reminding us to re-assess the rationality and reliability of its role of normalization factor for protein concentrations.

Figure 4C,D shows time-dependent curves of the peak area and peak height of the Phe band from 0 to 196 h, respectively, in which the change curve of the protein concentration is also plotted. For the sake of comparison, these curves are all normalized to their initial values. Unsurprisingly, the area and height curves both follow the similar trend as the protein concentration in supernatants. However, in the details, there are slight differences. The peak area of the Phe band initially essentially unchanged and then monotonically decreases with single exponential decay. The lag phase lasts up to ~16 h as shown in Figure 4C, and the attenuation rate is slower than that of the protein concentration. On the other hand, the variation of the Phe peak height maintains a mono-exponential decay from start to end. Although the decay rate is close to that of the concentration change, the lack of the lag phase indicates that it cannot reflect accurately the lysozyme concentration in the supernatant, especially in the early stage of incubation when the unfolding of protein tertiary structures occurs and the soluble oligomers are mostly formed. Given the unsatisfactory performance of the Phe indicator, using the Phe band intensity as the normalization factor for Raman spectroscopy is likely to lead to unpredictable errors, especially when discussing changes of the protein tertiary structures in the early stages of denaturation.

3.4 | The *p*H effect on the changes of HEWL tertiary structures

The *p*H value is a stressful inducer for protein denaturation. Using the Phe peak height at 1003 cm^{-1} as the normalization factor of Raman spectra, evolution kinetics of HEWL tertiary and secondary structures in the incubation conditions of 65°C and *p*H 2.0 were reported,[44] based on the recorded time-dependent indicators. However, the normalization factor was not reliable enough as mentioned above. Instead, the absorbance at 280 nm is a more perfect normalization factor for HEWL's Raman spectroscopy to remove the concentration effect. Herein, using the absolute absorbance at 280 nm as new normalization factor, we re-measured Raman spectroscopy of the denaturing HEWL at three different *p*H values, 1.1, 1.9, and 2.7. By comparing evolution kinetics of the indicators under various *p*H conditions, the *p*H effect on the denaturation kinetics of lysozyme is uncovered.

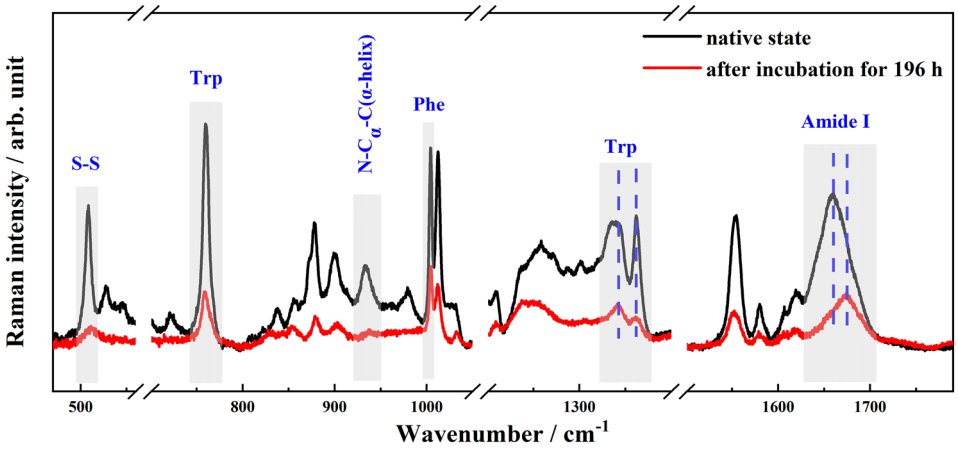

FIGURE 3 Raman spectra of the HEWL aqueous solution in the native state (in black) and the final state after incubation for 196 h involving mature fibrils (in red) with thermal and acidic treatments (65°C, *p*H 1.9), in the range of 480–1780 cm^{-1}. Major Raman indicators used in the text are marked.

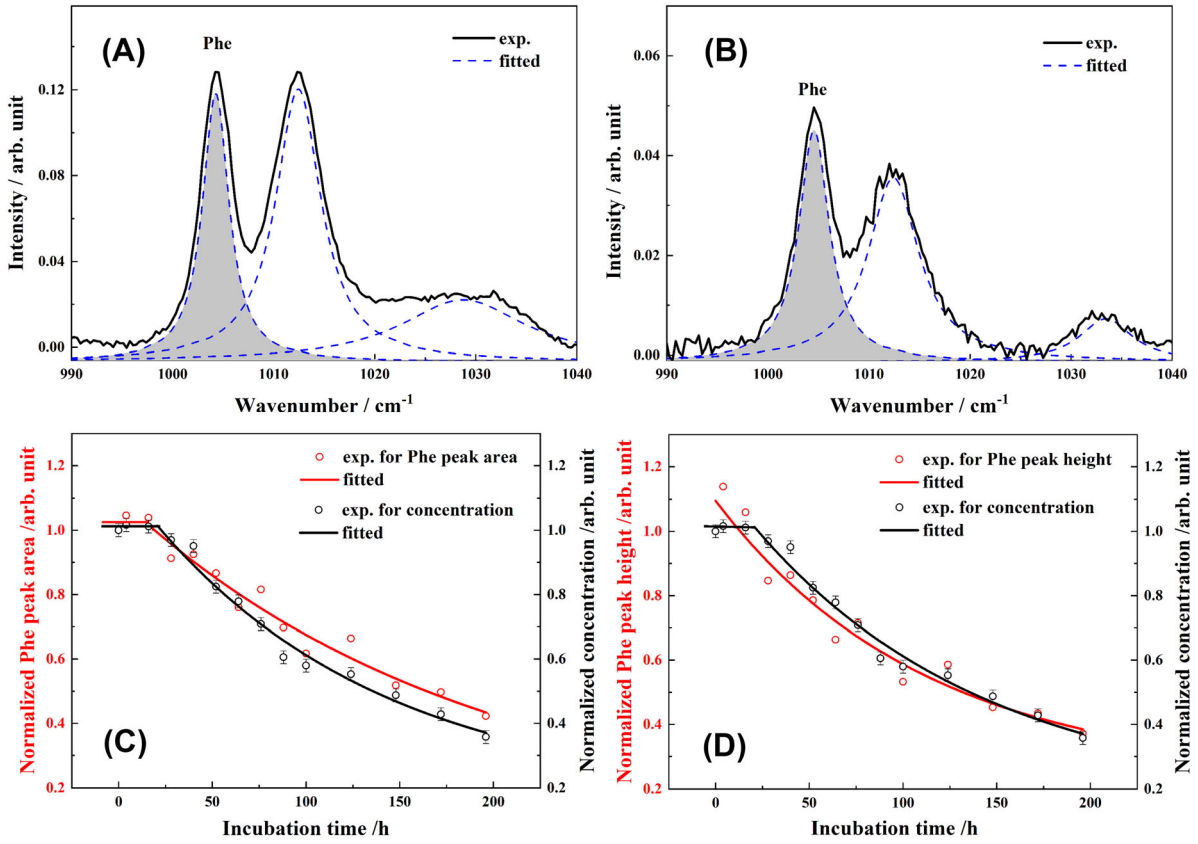

FIGURE 4 Partially magnified Raman spectra of lysozyme in the native state (A) and the final state after incubation for 196 h (B), and time-dependent curves of the corresponding relative area (C) and height (D) of the Phe peak, where the normalized concentration of protein in the supernatant is also plotted for comparison.

As listed in Table 1, two Trp vibrations and one S-S stretching band are sensitive indicators for conformational changes of protein tertiary structures. With tertiary structures unfolding, inner Trp residues will gradually be exposed to the aqueous medium. Figure 5A,B shows the consistent time-dependent curves of two Trp indicators, in which typically mono-exponential decay kinetics are observed at *p*H 1.1 and 1.9, whereas a very slow decay also existed at *p*H 2.7 but still far from the equilibrium state until 190 h, because of incomplete unfolding of protein tertiary structures. Such inefficient effect at *p*H 2.7 agrees with the previous experimental conclusion that significant transformation of HEWL structures only occurred at $pH < 2$.[17,21]

By fitting the curves with the single-exponential function, the decay rates are determined and listed in Table 2. Obviously, the rates of two Trp indicators are greatly consistent, whereas the S-S stretching indicator is nearly twice. Generally, local hydrophobic residues condense around the disulfide bonds through hydrophobic interactions to form the nucleus of a hydrophobic core of protein. Thus, when these disulfide bonds are broken, the hydrophobic residues, such as inner Trp residues, are gradually exposed to aqueous environment. In this way, the exposure rate of the Trp residues is rightly slower than that of disulfide bond breakage, although their initiation is synchronized. With increasing acidity, the unfolding rate of tertiary structures is significantly improved but nonlinearly dependent on the H^+ concentration. Additionally, a slightly blue shift of the S-S stretching peak position was observed with incubation time (Figure S4). Considering the peak position and bandwidth are affected by the distributions of various conformations of adjacent Cys residues forming the disulfide bonds, this blue shift implies the destruction of dominant disulfide bond conformations.

3.5 | The *p*H effect on the transformation of HEWL secondary structures

As shown in Figure 6A, the N-C_α-C intensity at 933 cm^{-1}, as a sensitive indicator for the population of α-helical segments, is monotonously reduced with incubation time, indicating that the α-helical structures in the

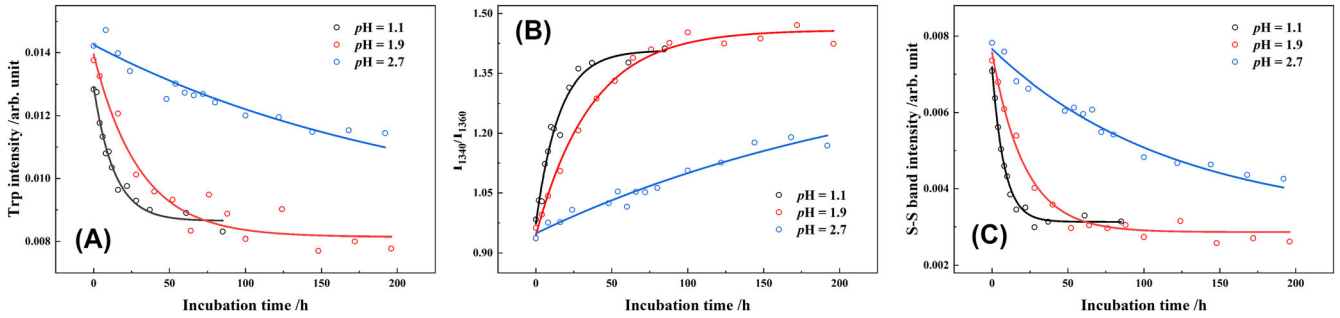

FIGURE 5 Time-dependence curves of the Trp band intensity at 759 cm^{-1} (A), the I_{1340}/I_{1360} indicator (B), and the S-S band intensity at 508 cm^{-1} (C), during thermal and acidic incubation.

TABLE 2 The single-exponential decay rate of Raman indicators for HEWL at three *p*H conditions, in the unit of h^{-1}.

*p*H	$[H^+]$ $(mol \cdot L^{-1})$	Trp intensity at 759 cm^{-1}	I_{1340}/I_{1360}	S-S band intensity at 508 cm^{-1}	N-C_α-C intensity at 933 cm^{-1}
1.1	79.4×10^{-3}	0.070 ± 0.010	0.065 ± 0.009	0.126 ± 0.007	0.12 ± 0.01
1.9	12.6×10^{-3}	0.033 ± 0.007	0.028 ± 0.002	0.046 ± 0.004	0.047 ± 0.007
2.7	2.0×10^{-3}	0.0045 ± 0.0004	0.004 ± 0.0003	0.0084 ± 0.0006	0.0061 ± 0.0006

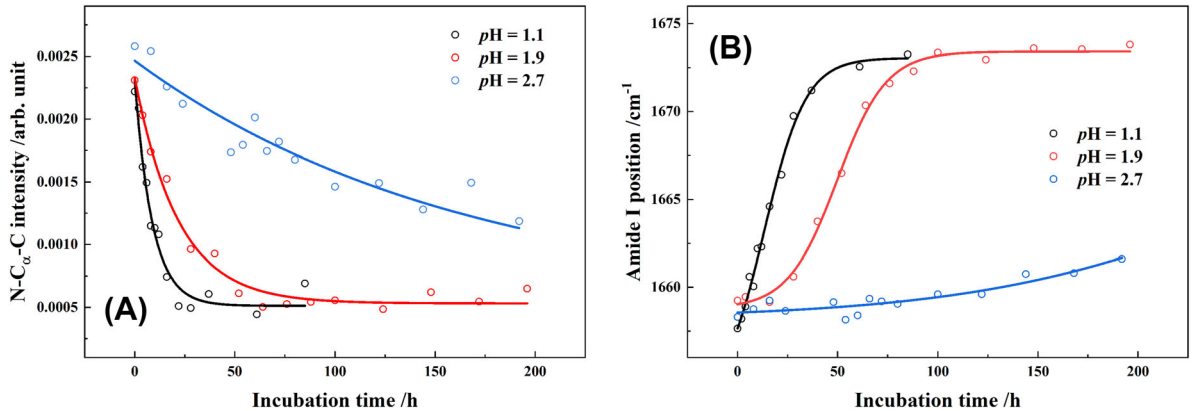

FIGURE 6 Time-dependence curves of the N-C_α-C band intensity at 933 cm^{-1} (A) and the peak position of the amide I band (B), during thermal and acidic incubation.

native HEWL are significantly disrupted. By fitting the curves, we obtained the corresponding decay rates under three *p*H conditions and listed them in Table 2. To our surprise, the rate is almost identical to that of the disulfide bond band at each *p*H value. This consistence strongly implies that the transformation of the HEWL α-helical structures occurs simultaneously with the disulfide bond breakage.

The peak position of the amide I band is another commonly used indicator for the transformation of protein secondary structures. For HEWL, various secondary structures have different peak positions in the amide I region,[55] for example, α-helical structures cover 1650–1660 cm^{-1},[56] organized β-sheets are mainly located at 1660–1670 cm^{-1},[44] β-turns and random structures are in 1670–1680 cm^{-1},[57] and random coils and small segments connecting various helices contribute the intensity at lower than 1650 cm^{-1}.[58,59] As proposedly previously,[44] α-helix prefers to transform into statistical coils as intermediates and subsequently form organized β-sheets. As a

TABLE 3 The lag duration (T_0), transition midpoint time (T_m), equilibrium duration (T_e), and a half interval (ΔT) of the amide I peak position at three *p*H conditions, in the unit of hour.

*p*H	T_0	T_m	T_e	ΔT
1.1	<2	13	35	10
1.9	25	50	76	12
2.7	~100	-	-	-

result, its incubation time-dependent curve always exhibits a sigmoid-function form, that is, a lag phase followed by a rapid growth stage and an equilibrium phase. Figure 6B exhibits the time-dependent curves in three *p*H conditions. Obviously, blue shift is distinctly observed for the amide I peak position with protein denaturation (Figure S5), validating the HEWL secondary structure transformation from α-helical to β-sheets.

To quantitatively compare the *p*H-dependent kinetics, the lag duration (T_0) and equilibrium duration (T_e) are determined through the curve-fitting with the sigmoid function, $P = P_D + \frac{P_N - P_D}{1+exp(\frac{T-T_m}{\Delta T})}$, where P_N and P_D are the peak positions of initial and final states, respectively, T_m is the transition midpoint time, and $2 \times \Delta T$ is the transition interval, and listed in Table 3. Notably, in the *p*H 2.7 condition, the protein denaturation is too slow to reach the equilibrium state until 196 h. Thus, only lag duration of ~100 h was observed in experiments. In the *p*H 1.9 solution, the lag phase lasts 25 h followed by a growth phase, and the equilibrium is achieved at 76 h. When the *p*H value decreases to 1.1, the transformation kinetics is significantly accelerated. As a result, the lag duration is shortened to less than 2 h, and the equilibrium state is obtained after 35 h. Meanwhile, the growth rate is also obviously improved according to the reduced ΔT with the H^+ concentration increasing.

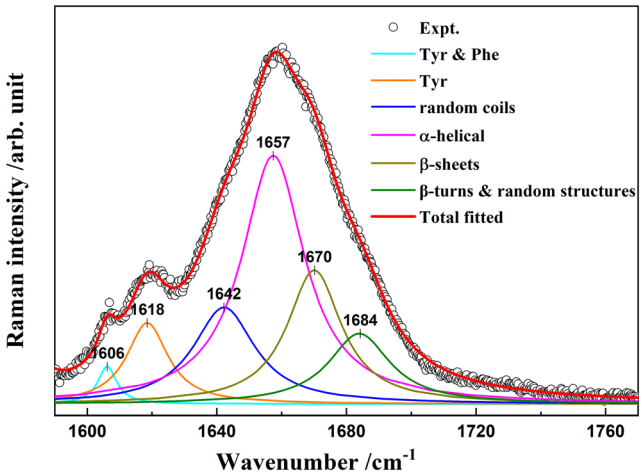

FIGURE 7 Experimental and fitted amide I band of HEWL in the native state under the *p*H 1.9 condition.

To further determinate the populations of various protein secondary structures at different *p*H values, a multi-peak fitting was performed for the amide I band profile at specific incubation times as done previously,[38,60] in which each Lorentzian-type peak represents one component. Figure 7 exhibits the result for the native HEWL in the *p*H 1.9 condition, where the two peaks with centers at 1618 and 1606 cm^{-1} are attributed to the Y1 mode of Tyr and the combined band of the Tyr Y2 and the Phe F1 modes, respectively.[40,61] The relative populations of dominant secondary structures at a specific time are summarized in Table 4, and the comparison between the experimental and fitted Raman spectra at specific incubation time is shown in Figure S6.

As shown in Table 4, the HEWL secondary structures dominantly consist of α-helix (47%) and a certain amount of β-sheet (22%) in the native state. Along incubation, the

TABLE 4 Curve-fitting analysis of the amide I Raman band profile of HEWL for different pH at the specific incubation times, together with the distribution percentages (area A%).

		α-Helix		Organized β-sheets		β-Turns & random structures		Random coils & small segments	
***p*H**	**Time/h**	**Position/cm^{-1}**	**A%**	**Position/cm^{-1}**	**A%**	**Position/cm^{-1}**	**A%**	**Position/cm^{-1}**	**A%**
1.1	0	1656	48	1671	23	1685	12	1640	17
	12	1655	40	1671	24	1685	22	1642	14
	28	1657	24	1672	40	1685	22	1640	14
	85	1657	21	1672	47	1687	21	1643	11
1.9	0	1657	47	1670	22	1684	13	1642	18
	28	1657	39	1672	25	1687	19	1643	17
	64	1657	27	1672	37	1685	23	1642	13
	196	1657	21	1673	48	1687	24	1641	7
2.7	0	1656	47	1668	22	1683	12	1640	19
	66	1657	43	1670	23	1685	12	1642	22
	122	1658	40	1671	21	1685	17	1643	22
	192	1657	36	1670	26	1685	19	1643	19

contributions of organized β-sheets, together with β-turns and random structures, are markedly improved with the reduction of α-helix. In the final state, the HEWL secondary structures dominantly consist of α-helix (21%), organized β-sheets (47%), and disordered structures including β-turns and random structures, and random coils and small segments (32%) at *p*H 1.1, and the almost identical populations are observed at *p*H 1.9 as α-helix (21%), organized β-sheets (48%), and disordered structures (31%). Thus, the $[H^+]$ concentration in the range of *p*H 1.1–1.9 has an insignificant influence on secondary structure distributions of the final-state HEWL.

It is well-known that low molecular weight oligomers formed during the early incubation can further assemble to amyloid fibril-like aggregates, labeled as "on-pathway," or gel-like products that are so-called "off-pathway."[53,60] As the oligomers have higher toxicity compared with mature fibrils, the "on-pathway" oligomeric intermediates are potential targets for therapeutic strategies aimed at interrupting the fibril formation. However, it is extremely difficult to distinguish the "on-pathway" or "off-pathway" intermediates in spectroscopy because they all have less ordered structures. Therefore, the distributions of amyloid fibrils and gel-like aggregates in the final state of protein amyloid fibrillation kinetics can provide direct clues for assessing the impact of a specific condition on the branching ratios of "on-pathway" and "off-pathway." In the current system, our above results strongly indicate that the branching ratios of "on-pathway" to amyloid fibrils and "off-pathway" to gel-like aggregates are independent on acidity in the *p*H 1.1–1.9 range, although the structure transformation rates are different.

4 | CONCLUSIONS

The normalized factor for Raman spectroscopy is vital for understanding precisely the denaturation kinetics of proteins through well-known Raman indicators. In this study, we compared two normalization factors for Raman spectra in amyloid fibrillation kinetics of lysozyme with thermal and acidic treatments, that is, the UV–vis absorbance at 280 nm and the Phe Raman band intensity. As the former shows the better consistence with the protein concentration in supernatants, the absorbance at 280 nm is thought as an excellent normalization factor for Raman spectra.

Using this new normalization factor, we performed a study of the *p*H effect on the transformation of HEWL tertiary and secondary structures by Raman spectroscopy. With increasing acidity, the unfolding of tertiary structures is significantly accelerated. Interestingly, the breaking of disulfide bonds occurs preferentially relative to the exposure of inside Trp residues, as its rate is approximately twice of the decay rates of Trp indicators. Moreover, the destruction rate of α-helical structures is almost identical to that of disulfide bonds regardless of *p*H values. In addition, a positive effect of the H^+ concentration on the transformation rates of HEWL secondary structures is confirmed; however, the populations of major secondary structure components in the final state remain in the *p*H < 2.0 solutions. Our results strongly indicate that the branching ratios of "on-pathway" to amyloid fibrils and "off-pathway" to gel-like aggregates are independent on the *p*H values in the range of 1.1–1.9.

ACKNOWLEDGMENTS

This work was financially supported by the National Natural Science Foundation of China (Nos. 22073088 and 22027801) and the National Key Research and Development Program of China (No. 2022YFF0707202).

ORCID

Xiaoguo Zhou https://orcid.org/0000-0002-0264-0146

REFERENCES

[1] A. S. De Toma, S. Salamekh, A. Ramamoorthy, M. H. Lim, *Chem. Soc. Rev.* **2012**, *41*, 608.
[2] F. Chiti, C. M. Dobson, *Annu. Rev. Biochem.* **2017**, *86*, 27.
[3] P. Alam, K. Siddiqi, S. K. Chturvedi, R. H. Khan, *Int. J. Biol. Macromol.* **2017**, *103*, 208.
[4] I. Shcherbatykh, D. O. Carpenter, *J. Alzheimer's Dis.* **2007**, *11*, 191.
[5] C. Ha, J. Ryu, C. B. Park, *Biochemistry* **2007**, *46*, 6118.
[6] S. Bolognin, L. Messori, P. Zatta, *NeuroMol. Med.* **2009**, *11*, 223.
[7] P. Faller, C. Hureau, O. Berthoumieu, *Inorg. Chem.* **2013**, *52*, 12193.
[8] B. Ma, F. Zhang, X. Wang, X. Zhu, *Int. J. Biol. Macromol.* **2017**, *98*, 717.
[9] S. Ghosh, N. K. Pandey, S. Bhattacharya, A. Roy, N. V. Nagy, S. Dasgupta, *Int. J. Biol. Macromol.* **2015**, *76*, 1.
[10] S. Ghosh, S. Mondal, S. Das, R. Biswas, *Fluid Phase Equilib.* **2012**, *332*, 1.
[11] E. House, J. Collingwood, A. Khan, O. Korchazkina, G. Berthon, C. Exley, *J. Alzheimer's Dis.* **2004**, *6*, 291.
[12] G. F. Kwakye, M. M. B. Paoliello, S. Mukhopadhyay, A. B. Bowman, M. Aschner, *Int. J. Environ. Res. Public Health* **2015**, *12*, 7519.
[13] A. B. Bowman, G. F. Kwakye, E. Herrero Hernández, M. Aschner, *J. Trace Elem. Med. Biol.* **2011**, *25*, 191.
[14] S.-Y. Ow, D. E. Dunstan, *Soft Matter* **2013**, *9*, 9692.
[15] V. A. Shashilov, I. K. Lednev, *J. Am. Chem. Soc.* **2008**, *130*, 309.
[16] S. E. Hill, J. Robinson, G. Matthews, M. Muschol, *Biophys. J.* **2009**, *96*, 3781.
[17] L. N. Arnaudov, R. de Vries, *Biophys. J.* **2005**, *88*, 515.
[18] R. Swaminathan, V. K. Ravi, S. Kumar, M. V. S. Kumar, N. Chandra In, *Advances in protein chemistry and structural biology*, Academic Press, United Kingdom **2011**.

[19] K. Al Adem, S. Lukman, T. Y. Kim, S. Lee, *Int. J. Biol. Macromol.* **2020**, *149*, 921.
[20] S. Venkataramani, J. Truntzer, D. R. Coleman, *J. Pharm. Bioallied Sci* **2013**, *5*, 148.
[21] E. N. Lewis, W. Qi, L. H. Kidder, S. Amin, S. M. Kenyon, S. Blake, *Molecules* **2014**, *19*, 20888.
[22] L. C. Burnett, B. J. Burnett, B. Li, S. T. Durrance, S. Xu, *Open J. Biophys.* **2014**, *4*, 39.
[23] D. Chalapathi, A. Kumar, P. Behera, S. N. Sathi, R. Swaminathan, C. Narayana, *Molecules* **2022**, *27*, 7122.
[24] R. Rajan, S. Ahmed, N. Sharma, N. Kumar, A. Debas, K. Matsumura, *Mater. Adv.* **2021**, *2*, 2.
[25] V. Sereda, I. K. Lednev, *J. Raman Spectrosc.* **2014**, *45*, 665.
[26] D. Kurouski, R. P. Van Duyne, I. K. Lednev, *Analyst* **2015**, *140*, 4967.
[27] T. Deckert-Gaudig, V. Deckert, *Sci. Rep.* **2016**, *6*, 6.
[28] M. Tabatabaei, F. A. Caetano, F. Pashee, S. S. G. Ferguson, F. Lagugné-Labarthet, *Analyst* **2017**, *142*, 4415.
[29] R. A. Karaballi, S. Merchant, S. R. Power, C. L. Brosseau, *Phys. Chem. Chem. Phys.* **2018**, *20*, 4513.
[30] E. Li-Chan, S. Nakai, *J. Agric. Food Chem.* **1991**, *39*, 1238.
[31] H. Takeuchi, *Biopolymers* **2003**, *72*, 305.
[32] V. Kocherbitov, J. Latynis, A. Misiūnas, J. Barauskas, G. Niaura, *J. Phys. Chem. B* **2013**, *117*, 4981.
[33] Z.-Q. Wen, *J. Pharm. Sci.* **2007**, *96*, 2861.
[34] T. G. Spiro, B. P. Gaber, *Annu. Rev. Biochem.* **1977**, *46*, 553.
[35] R. C. Lord, N. T. Yu, *J. Mol. Biol.* **1970**, *50*, 509.
[36] M. Tsuboi, M. Suzuki, S. A. Overman, G. J. Thomas, *Biochemistry* **2000**, *39*, 2677.
[37] D. I. Ellis, D. P. Cowcher, L. Ashton, S. O'Hagan, R. Goodacre, *Analyst* **2013**, *138*, 3871.
[38] S. Dolui, A. Mondal, A. Roy, U. Pal, S. Das, A. Saha, N. C. Maiti, *J. Phys. Chem. B* **2020**, *124*, 50.
[39] L. Xing, K. Lin, X. Zhou, S. Liu, Y. Luo, *J. Phys. Chem. B* **2016**, *120*, 10660.
[40] B. Hernández, F. Pflüger, S. G. Kruglik, M. Ghomi, *J. Raman Spectrosc.* **2013**, *44*, 827.
[41] N. Howell, E. Li-Chan, *International Journal of Food Science & Technology* **1996**, *31*, 439.
[42] A. M. Herrero, M. I. Cambero, J. A. Ordóñez, L. de la Hoz, P. Carmona, *Food Chem.* **2008**, *109*, 25.
[43] A. M. Herrero, P. Carmona, S. Cofrades, F. Jiménez-Colmenero, *Food Research International* **2008**, *41*, 765.
[44] L. Xing, W. Fan, N. Chen, M. Li, X. Zhou, S. Liu, *J. Raman Spectrosc.* **2019**, *50*, 629.
[45] V. Shashilov, M. Xu, V. V. Ermolenkov, L. Fredriksen, I. K. Lednev, *J. Am. Chem. Soc.* **2007**, *129*, 6972.
[46] L. Xing, N. Chen, W. Fan, M. Li, X. Zhou, S. Liu, *Int. J. Biol. Macromol.* **2019**, *132*, 929.
[47] W. Fan, L. Xing, N. Chen, X. Zhou, Y. Yu, S. Liu, *The Journal of Physical Chemistry B* **2019**, *123*, 8057.
[48] A. M. Herrero, P. Carmona, S. Cofrades, F. Jimenez-Colmenero, *Food Research International* **2008**, *41*, 765.
[49] A. M. Herrero, M. I. Cambero, J. A. Ordonez, L. De la Hoz, P. Carmona, *Food Chem.* **2008**, *109*, 25.
[50] N. Howell, E. LiChan, *Int. J. Food Sci. Technol.* **1996**, *31*, 439.
[51] W. Wang, Y. J. Wang, D. Q. Wang, *Int. J. Pharm.* **2008**, *347*, 31.
[52] S. Ghosh, N. K. Pandey, S. Bhattacharya, A. Roy, S. Dasgupta, *Int. J. Biol. Macromol.* **2012**, *51*, 1.
[53] X. Chen, L. Xing, X. Li, N. Chen, L. Liu, J. Wang, X. Zhou, S. Liu, *ACS Omega* **2023**, *8*, 16439.
[54] G. A. Eberlein, P. R. Stratton, Y. J. Wang, *PDA J. Pharm. Sci. Technol.* **1994**, *48*, 224.
[55] N. Kuhar, S. Sil, S. Umapathy, *Spectrochim. Acta, Part a* **2021**, *258*, 119712.
[56] T. J. Yu, J. L. Lippert, W. Peticola, *Biopolymers* **1973**, *12*, 2161.
[57] A. Barth, C. Zscherp, *Q. Rev. Biophys.* **2002**, *35*, 369.
[58] K. Murayama, M. Tomida, *Biochemistry* **2004**, *43*, 11526.
[59] M.-J. Paquet, M. Laviolette, M. Pézolet, M. Auger, *Biophys. J.* **2001**, *81*, 305.
[60] L. Liu, X. Li, N. Chen, X. Chen, L. Xing, X. Zhou, S. Liu, *Spectrochim. Acta, Part a* **2023**, *296*, 122650.
[61] W. B. Fischer, H. H. Eysel, *Spectrochim. Acta, Part a* **1992**, *48*, 725.

SUPPORTING INFORMATION

Additional supporting information can be found online in the Supporting Information section at the end of this article.

How to cite this article: D. Liu, N. Chen, T. Zhang, X. Zhou, S. Liu, *J Raman Spectrosc* **2024**, *55*(7), 787. https://doi.org/10.1002/jrs.6674